

1 Differentiating between crop and soil effects on soil moisture 2 dynamics

3 Helen Scholz¹, Gunnar Lischeid^{2,3}, Lars Ribbe¹, Ixchel Hernandez Ochoa⁴, Kathrin Grahmann²

4 ¹Institute for Technology and Resources Management in the Tropics and Subtropics (ITT), TH Köln, Cologne, Germany

5 ²Leibniz Centre for Agricultural Landscape Research (ZALF), Müncheberg, Germany

6 ³Institute for Environmental Sciences and Geography, University of Potsdam, Potsdam, Germany

7 ⁴Institute of Crop Science and Resource Conservation (INRES), Crop Science Group, University of Bonn, Bonn, Germany

8 *Correspondence to:* kathrin.grahmann@zalf.de

9 **Abstract.** There is urgent need to develop sustainable agricultural land use schemes. Intensive crop production has induced
10 increased greenhouse gas emissions and enhanced nutrient and pesticide leaching to groundwater and streams. Climate change
11 is also expected to increase drought risk as well as the frequency of extreme precipitation events in many regions.
12 Consequently, sustainable management schemes require sound knowledge of site-specific soil water processes that explicitly
13 take into account the interplay between soil heterogeneities and crops. In this study, we applied a principal component analysis
14 to a set of 64 soil moisture time series from a diversified cropping field featuring seven distinct crops and two weeding
15 management strategies.

16 Results showed that about 97% of the spatial and temporal variance of the data set was explained by the first five principal
17 components. Meteorological drivers accounted for 72.3% of the variance, 17.0% was attributed to different seasonal behaviour
18 of different crops. While the third (4.1%) and fourth (2.2%) principal component were interpreted as effects of soil texture and
19 cropping schemes on soil moisture variance, respectively, the effect of soil depth was represented by the fifth component
20 (1.7%). However, neither topography nor weed control had a significant effect on soil moisture variance. Contrary to common
21 expectations, soil and rooting pattern heterogeneity seemed not to play a major role. Findings of this study highly depend on
22 local conditions. However, we consider the presented approach generally applicable to a large range of site conditions.

23 1 Introduction

24 Agriculture plays a major role to ensure the provision of food to a growing global population. At the same time, climate change
25 is putting yield stability at risk due to extreme weather events, rising the need for sustainable management of resources, such
26 as water and soil (Trnka et al., 2014). The transformation from large homogeneously cropped fields towards diversified
27 agricultural landscapes has been identified as an opportunity that can contribute to climate adaptation due to the positive effects
28 on multiple ecosystem services (Tamburini et al., 2020), and cropping system resilience to climatic extremes (Birtal and
29 Hazrana, 2019). Additionally, crop diversification is highly beneficial by reducing soil erosion through permanent soil cover
30 (Paroda et al., 2015), and by improving resource use efficiency through wider crop rotations (Rodriguez et al., 2021).

31 In terms of soil water dynamics, crop and management diversification can lead to improved water-stable macro-aggregation,
32 reduced soil compaction and increased soil organic carbon, which can reduce soil water infiltration and improve water retention
33 (Alhameid et al., 2020; Fischer et al., 2014; Karlen et al., 2006; Koudahe et al., 2022; Nunes et al., 2018). Korres et al. (2015)
34 reported that spatial variability of soil moisture was mainly driven by soil characteristics, followed by crop cover and
35 management. Soil moisture is also affected by soil texture and pore size distribution (Krauss et al., 2010; Rossini et al., 2021;
36 Pan and Peters-Lidard, 2008). The quantification of the impact of these effects on soil moisture variability is important, for
37 instance for hydrological applications and adopted management practices in agriculture (Hupet and Vanclooster, 2002).
38 As the diversity of independent variables in agricultural systems increases, demands for frequency and spacing of soil moisture
39 measurements and related data interpretation grow. Therefore, soil sensor networks are receiving increased attention,
40 particularly in Precision Agriculture (PA; Bogen et al., 2022; Salam and Raza, 2020), where the main goal is to increase
41 efficiency and productivity at the farm level while minimizing the negative impacts on the environment (Taylor and Whelan,
42 2010). Soil sensor networks can meaningfully contribute to PA as they can be used for various purposes, including the
43 delineation of management zones (Khan et al., 2020; Salam and Raza, 2020). Still, one of the most important demands to be
44 fulfilled by soil sensor networks is soil moisture monitoring, as accurate measurement of soil water content can play an
45 important role in improving water management and therefore, crop yields (Salam, 2020).
46 Wireless solutions, for instance based on LoRaWAN (Long Range Wide Area Network) technology, in combination with
47 electromagnetic soil moisture sensors avoid labour-intensive and destructive soil moisture measurements that disrupt field
48 traffic. The development of such wireless sensor networks (WSN) enables broad and affordable application also in areas with
49 low cellular coverage (Cardell-Oliver et al., 2019; Lloret et al., 2021; Placidi et al., 2021; Prakosa et al., 2021).
50 The evolution of WSN does not only have benefits for management but is also of high relevance for fostering the
51 understanding of hydrological dynamics in the vadose zone. High-resolution datasets measured under real farming conditions
52 can be used to characterize and analyse spatio-temporal dynamics of soil water. Due to the large size of data sets that are
53 recorded with WSN, sophisticated data analysis approaches are required to detect hidden patterns and determine influence
54 factors on soil moisture variability (Vereecken et al., 2014). With the introduction of multiple-points geostatistics, it became
55 possible to not only analyse patterns but also connect them with factors affecting soil moisture, such as topography, texture,
56 crop growth and water uptake, and land management (Brocca et al., 2010; Strebelle et al., 2003). Wavelet analysis can analyse
57 both localized features as well as spatial trends through which non-stationary variation of soil properties can be considered (Si,
58 2008). Cross-correlation analysis allowed linking soil moisture variability to climatic variables (Mahmood et al., 2012).
59 Furthermore, temporal stability analyses detect spots in the investigated area which are consistently wetter or drier than the
60 mean soil moisture (Baroni et al., 2013; Vachaud et al., 1985; Vanderlinden et al., 2012). This method was already successfully
61 used to detect soil moisture patterns related to soil properties, vegetation, and topography (Zhao et al., 2010).
62 Principal component analysis (PCA) is another method that was successfully applied for soil moisture variability analysis at
63 the field (Hohenbrink et al., 2016; Hohenbrink and Lischeid, 2015; Martini et al., 2017), catchment (Korres et al., 2010;
64 Lischeid et al., 2017; Nied et al., 2013; Graf et al., 2014), and regional (Joshi and Mohanty, 2010) scale. These studies build

65 on previous applications in climatology where the term “Empirical Orthogonal Functions” is used (Bretherton et al., 1992) and
66 are examples for how space and time dimensions can be disentangled and assigned to influencing factors. Additionally, the
67 propagation of hydrological signals (e.g. precipitation events) over depth can be assessed (Hohenbrink et al., 2016). This opens
68 up great opportunities to improve the knowledge of changing soil water dynamics in complex diversified agricultural systems
69 with increasing heterogeneity (e. g. soil texture) and site-specific adjustment of crop and field management which, to our
70 knowledge, have hardly been studied so far. The main objective of this study was to identify the drivers of soil moisture
71 variability in a diversified cropping agricultural field in terms of soil texture, crop selection and field management by applying
72 PCA. Special foeusemphasis was putgiven on the interpretation of spatial and temporal effects of crop diversification and of
73 soil heterogeneities on soil moisture dynamics.

74 For this, we analysed a high-resolution soil moisture data set measured by a novel underground LoRaWAN monitoring system
75 with soil moisture sensors in different depths of the vadose zone at a spatial-temporally diversified agricultural field in
76 Northeast Germany. The novelty of this WSN relies on its unique on-farm installation environment. The deployment of
77 transmission units in 0.3 m soil depth and 180 sensors in up to 0.9 m soil depth; allows high spatio-temporal resolution wireless
78 data transmission, and enables conventional farming practices like machinery traffic, tillage and mechanical weeding.

79 **2 Materials and methods**

80 **2.1 Study site**

81 The study site (52°26'51.8"N 14°08'37.7"E, 66-83 m.a.s.l.) is located near the city of Müncheberg in the federal state of
82 Brandenburg in Northeastern Germany. The landscape is classified as a hummocky ground moraine that formed during the
83 last glacial periods. Glacial and interglacial processes as well as subsequent erosion resulted in highly heterogeneous soils
84 (Deumlich et al., 2018), being classified as Dystric Podzoluvisols according to the FAO scheme (Fischer et al., 2008). In the
85 top 0.3 m soil layer, total organic carbon was 0.94% and total nitrogen content was 0.07%, and pH was 6.12. Between January
86 1991 and December 2020, the mean annual temperature in Müncheberg was 9.6°C, and the mean annual sum of precipitation
87 was 509 mm (DWD Climate Data Center (CDC), 2021).

88 **2.2 Experimental setup**

89 The data collection was carried out from December 2020 until mid of August 2021 in the patchCROP experiment (Grahmann
90 et al, 2021; Donat et al., 2022). This landscape experiment has been set up to study the multiple effects of cropping system
91 diversification on productivity, crop health, soil quality, and biodiversity. To that end, a cluster analysis was carried out based
92 on soil maps and multi-year (2010 to 2019) yield data to identify high and low yield potential zones in the 70-ha large field
93 (Donat et al., 2022). Afterwards, single experimental units comprising 30 patches with an individual size of 0.52 ha (72 m ×
94 72 m) each, have been implemented in both, high and low yield potential zones where each of those zones is characterized by
95 varying soil conditions and a site-specific five-year, legume-based crop rotation (Grahmann et al., 2021). The remaining area

96 outside of the 30 patches was planted with winter rye. For the current study, twelve out of 30 patches were considered (Table
97 1, Figure 1). Specific patches were selected to capture the soil heterogeneities in terms of soil texture, but also the seasonal
98 patterns of the crop rotation that may have important effects on the soil water dynamics such as crop types, presence of cover
99 crops or fallow periods. In the cropping season 2020/2021, seven different main crops were grown. For subsequent data
100 interpretation, crops have been grouped into A) winter crops, B) fallow, followed by summer crops and C) cover crops,
101 followed by summer crops. In seven out of twelve considered patches, weed control was carried out with herbicide application,
102 referred as “conventional” pesticide application, while in the remaining five patches, “reduced” pesticide management was
103 carried out by mainly using mechanical weeding, by harrowing, blind harrowing, and hoeing. Only in the case of high weed
104 pressure herbicides were applied. Due to the potential impact of mechanical weeding, i.e., on rainwater infiltration, soil
105 evaporation and topsoil rooting intensity, we differentiate between these modes of weed control.

106 **2.3 Data collection**

107 **2.3.1 Soil moisture data**

108 Soil moisture was recorded by a long-range-wide-area network (LoRaWAN) based WSN. In each patch, one Dribox box
109 equipped with a SDI-12 distributor (serial data interface at 1200 baud rate, TBS04, TekBox, Saigon, Vietnam) connected to
110 six TDR-sensors (TDR310H, Acclima, Meridian, USA) and attached to an outdoor remote terminal unit (RTU) fully
111 LoRaWAN compliant (TBS12B: 4+1 channel analogue to SDI-12 interface for 24 Bit A/D conversion of sensor signals,
112 TekBox, Saigon, Vietnam) was installed as LoRa node. It was deployed at least 0.3 m below ground to allow field traffic and
113 soil tillage. The sensors and boxes were installed between August and November 2020. At two georeferenced locations within
114 each patch, soil moisture sensors were installed in 0.3, 0.6 and 0.9 m depth, respectively. Sensors were approximately 2 m
115 apart from the LoRa node in angles between 45° and 60° (Figure 1). Soil moisture sensors at 0.3 m were placed horizontally,
116 while sensors at 0.6 and 0.9 m depth were placed vertically using auger-made boreholes and extension tubes for soil insertion.
117 Communication of LoRa nodes was wireless and autarkic in energy supply. Thus, no electric cabling except from connections
118 between sensors and LoRa nodes was needed. Under optimum conditions, battery running time of the LoRa nodes can be up
119 to 12 months but can be reduced to 8 months when radio transmission is attenuated (e.g. due to near water-saturated soil)
120 which then increases power consumption (Bogena et al., 2009). Data was recorded every 20 minutes by the LoRa nodes
121 through a LoRa-WAN Gateway DLOS8 (UP GmbH, Ibbenbüren, Germany) which was equipped with the modem TL-
122 WA7510N (TP Link, Hong Kong, China) to transfer the data to a cloud from where collected data could be accessed directly
123 after the measurement. The time series included in this study covered the period from December 01, 2020, until August 14,
124 2021 (Figure 2).

125 **2.3.2 Weather data**

126 Precipitation and temperature data (Figure 3) with a 15 min temporal resolution were obtained from two weather stations
127 located in the Eastern and Western end of the main patchCROP field. Climatic water balance was calculated from precipitation
128 and potential evapotranspiration, both measured at the climate station by the German Weather Service in Müncheberg (DWD
129 Climate Data Center (CDC), 2021). This station was chosen due to its proximity to the study site.

130 **2.3.3 Remotely sensed data for vegetation dynamics**

131 Furthermore, drone imagery from May 20, 2021, May 31, 2021, and July 06, 2021, was used for vegetation assessment. The
132 drone fixed-wing UAV-based RS eBee platform (SenseFly Ltd., Cheseaux-Lausanne, Switzerland) was operated at noon time
133 and recorded multispectral imagery with a Parrot Sequoia+ camera (green, red, NIR, and red edge bands, spatial resolution of
134 0.105 m) and thermal imagery of the surface (only on May 31, 2021) with a senseFly Duet T camera with a spatial resolution
135 of 0.091 m (Table 2). The multispectral imagery was processed with Pix4D to obtain the Normalized Difference Vegetation
136 Index (NDVI), following Eq. (1):

$$137 \quad NDVI = \frac{NIR-Red}{NIR+Red} \quad (1)$$

138 in which NIR is the intensity of reflected near-infrared light (reflected by vegetation) and Red the intensity of reflected red
139 light (absorbed by vegetation). A digital elevation model with a spatial resolution of 1 m (GeoBasis-DE and LGB, 2021) was
140 used to calculate the slope (ArcGIS 10.7.0; ESRI, 2011) (Table 2).

141 **2.3.4 Soil information**

142 *Soil texture by layer*

143 Manual classification of soil texture by layer was carried out by collecting 140 samples in eight of twelve analysed patches.
144 Samples were taken with a 1 m-length Pürckhauer soil auger. Soil sampling points were located between 0.8 m and 2.5 m
145 away from the soil moisture sensors to minimize damage risk. Soil textural class was manually determined at the field by
146 applying the protocol “Finger test to determine soil texture according to DIN 19682-2 and KA5” (Sponagel et al., 2005).
147 Additionally, representative soil samples were collected and analysed at the laboratory to determine particle size distribution
148 for sand, silt, and clay (soil texture based on the German particle classification). Soil texture was analysed following the DIN
149 ISO 11277 (2002) reference method by wet sieving and sedimentation, using the SEDIMAT 4-12 (Umwelt-Geräte-Technik
150 GmbH, Germany). The sand fraction in this method is defined between 2 and 0.063 mm, according to IUSS Working Group
151 WRB (2015).

152 The laboratory soil texture analysis showed that soil texture variability increased with depth. In the third layer (average bottom
153 depth = 0.92 m), the sand and clay content across 133 sampling points varied between 53% to 94% and from 2% to 22%,
154 respectively. Also, soil texture was sandier in the low yield potential soil than in the high yield potential areas, even when

155 corresponding to the same soil textural class. Therefore, to extrapolate the laboratory-based soil particle distribution to the soil
156 textural classes manually determined at the field, the high and low yield potential laboratory samples were pooled separately.
157 The average soil particle distribution was calculated for each soil textural class within each yield potential. These values were
158 then assigned to the soil layer that had the respective soil textural class in the manual readings.

159 ~~To extrapolate the laboratory based soil particle distribution from the laboratory to the manual soil textural classes manually~~
160 ~~determined at the field, the high and low yield potential laboratory samples were pooled separately, and the average soil~~
161 ~~particle distribution was calculated by for each soil textural class was calculated and assigned to the respective soil layer with~~
162 ~~that specific particular soil textural class. The soil texture analysis showed that soil texture variability increased with depth. In~~
163 ~~the third layer (average bottom depth = 92 cm/0.92 m), the sand and clay share content across 133 sampling points varied~~
164 ~~between 53% to 94% and 2% to 22%, respectively. Soil samplesampling points were between located approximately 0.8 m~~
165 ~~and 2.5 m far away from the soil moisture sensors to minimize damage risk. The transferability of texture information from~~
166 ~~the sampling point to the sensor location was not ensured due to high nugget effects. Furthermore, manual soil texture analysis~~
167 ~~data were not available for all analysed patches. Consequently, they were not included into further correlation analysis.~~

168 ***Topsoil proximal~~ly~~ sensed data***

169 In October 2019, the “Geophilus” soil scanner system (Lueck and Ruehlmann, 2013) was used in the entire field to map soil
170 electrical resistivity (ERa) as a proxy for texture for the top soil, using reference soil samples to calibrate the readings. A total
171 of four georeferenced reference soil samples were taken until 0.25 m soil depth, and locations were selected based on the
172 proximal soil sensor data (sensor-guided sampling; Bönecke et al., 2021). The “Geophilus” system is based on sensor fusion
173 in which ERa sensors are coupled with a gamma-ray detector. Apparent electrical conductivity was measured by pulling one
174 or more sensor pairs mounted on wheels across the field where each pair of sensors measured a different soil depth. Amplitude
175 and phase were measured simultaneously using frequencies from 1 MHz to 1 kHz. Reference soil samples were analysed via
176 soil-particle size analysis according to DIN ISO 11277 (2002) and served as calibration information in order to estimate sand,
177 silt and clay content in the top 0.25 m soil for the entire field. A non-linear regression model was applied. The RMSE of sand
178 content (5.7%) was considerably smaller than the standard deviation of the sand content in the first layer from the manual soil
179 texture analysis (11.9%), indicating a satisfactory prediction performance. The gamma-sensor was used to minimize
180 uncertainties, being less sensitive to soil moisture than the ERa readings (Bönecke et al., 2021). The estimated sand content in
181 the upper 0.25 m at the study site varied between 69.1% and 81.2% and averaged 79.0% (Table 1, Figure 1).

182 **2.4 Data processing**

183 Soil moisture data were available at 20-minute intervals. Transmission failures due to discharged batteries, signal disturbances
184 after rainfall, in patches with a high density of biomass (e.g. maize), and theft of parts of the WSN led to data gaps that affected
185 in some cases all sensors of the WSN and amounted to 81 out of 257 days of the measuring period. The affected days were

186 therefore skipped for the analysis. Whereas time series of eight sensors were excluded due to a higher frequency of transmission
187 failures, in total, 64 time series were used for the analysis, and additional data gaps for single sensors were interpolated linearly.
188 Of all 20,668 interpolated gaps, 96% were shorter than two hours, 3% between two and six hours and 1% longer than six hours.
189 In 26 cases, gaps exceeded the duration of one day. The interpolation was justified as the differences between the values before
190 and after the gaps were within the measuring accuracy of 1 vol-% of the soil moisture sensors (Acclima Inc., 2019). As
191 indicated by the retailer, sensors might suddenly jump to a soil moisture value of 28.6% and go back to normal again after one
192 or few time steps. Thus, a data deletion procedure of abrupt jumps to 28.6 was created. Further minor spikes were not removed
193 since experience has shown that they do not significantly affect the results of PCA. To ensure equal weighting for the
194 subsequent analysis, all soil moisture time series were z-transformed to unit variance and zero mean each (cf. Hohenbrink and
195 Lischeid, 2015). As a consequence, differences of absolute values were not considered by the further analysis.

196 **2.54 Statistical analysis**

197 To identify common temporal patterns among single time series, the soil moisture data set was analysed by a principal
198 component analysis (PCA). In a first step, PCA decomposes the total variance of a multivariate data set into independent
199 fractions called principal components (PCs). The number of PCs is the same as the number of time series in the input data set.
200 Each PC consists of eigenvectors (loadings), scores, and eigenvalues. The scores reflect the temporal dynamics. The
201 importance of single principal components for single sites is represented by the loadings of each PC (Jolliffe, 2002; Lehr and
202 Lischeid, 2020). Loadings are the Pearson correlation coefficients of the single time series of the input data set with the scores
203 of each PC, respectively. The eigenvalues of the single PC are proportional to the variance that they explain. The PCs are
204 sorted in descending order of eigenvalues. Eigenvalues greater than one indicate that a PC explains more variance than -a
205 single input time series could contribute to the total variance of the entire input data set (Kaiser, 1960). More details on principal
206 component analysis for time series analysis are found in Jolliffe (2002). The PCA was performed using the *prcomp* function in
207 R version 4.1.0 (R Development Core Team, 2021).

208 The scores of the principal components constitute time series. Every observed soil moisture z-transformed time series can be
209 presented at arbitrary precision as a combination of various principal components. When the data set consists of time series of
210 the same observable measured at different locations, the first principal component describes the mean behaviour inherent in
211 the data set. Subsequent principal components reflect typical modifications of that mean behaviour at single locations due to
212 different effects. Thus, generating synthetic time series as linear combinations of the first PC and another additional PC helps
213 to assign this additional PC to a specific effect. To that end, scores of that component have either been added to or subtracted
214 from those of the first component using arbitrarily selected factors. The two resulting graphs show how the respective PC
215 causes deviations from the mean behaviour of the data set.

216 The relations to soil and vegetation parameters were tested by computing the Pearson correlation coefficients between the
217 scores and arithmetic mean values of all input time series as well as the Pearson correlation coefficients between loadings and
218 sand content until 0.25 m depth, sensor depth, antecedent z-transformed soil moisture, slope, and drone imagery products

219 (NDVI and surface temperature). Eventually, the Wilcoxon-Mann-Whitney test was applied to check whether loadings can be
220 grouped by management parameters (crops, cover crops, weeding management). All statistical analyses were conducted with
221 R version 4.1.0 (R Development Core Team, 2021).

222 **3 Results**

223 **3.1 Manual soil texture analysis**

224 The transferability of texture information from the sampling point to the soil moisture sensor location was not ensured due to
225 high nugget effects. Furthermore, manual soil texture analysis data were not available for all analysed patches. Consequently,
226 they were not included into further analysis.

227 **3.2 Principal component analysis**

228 The principal component analysis yielded five components with Eigenvalues exceeding one, which accounted for >97% of the
229 total variance of the data set (Table 3).

230 **3.2.1 First principal component**

231 The first principal component explained 72.3% spatiotemporal variance of the data set. All loadings on the first PC were
232 negative (Appendix A). The Pearson correlation coefficient of the scores of the first principal component with the mean values
233 of all input time series was less than - 0.999 ($p < 0.01$), the correlation between the scores and the cumulative climatic water
234 balance ($P - ET_p$) was -0.969 ($p < 0.01$). Thus, the time series of the negative scores of this component represented the mean
235 behaviour of soil moisture driven by external factors such as precipitation, temperature, and seasons in general which affected
236 time series in the same way, although to different degrees (cf., Hohenbrink et al., 2016; Lischeid et al., 2021).

237 **3.2.2 Second principal component**

238 The second principal component explained 17.0% of the total variance. The loadings ranged from -0.801 to 0.760 with a
239 median of -0.030 (Figure 4). The loadings showed a crop group specific pattern. All winter crops (barley, oats, rye) had positive
240 loadings with only one exception in 0.9 m depth. The summer crops maize, soy, and sunflower exhibited negative loadings. In
241 contrast, the summer crop lupine exhibited mostly positive loadings, similar to the winter crops, although of slightly smaller
242 magnitude. According to the Wilcoxon-Mann test, the group of barley, oats, rye, and lupine differed significantly from the
243 group of maize, soy, and sunflower.

244 As described in the Methods section, synthetic time series were generated as a linear combination of PC1 and PC2 (Figure 5).
245 The graph resulting from applying a positive factor for PC2 represents a typical deviation from mean behaviour for sites that
246 exhibit positive loadings, e.g., winter crops (blue line). The opposite holds for the summer crops which load negatively with
247 PC2 (orange line). Both lines plot very close to each other in February and March. In contrast, the orange line shows lower

248 values than the blue line in December and January, indicating lower soil moisture at the summer crop patches. The inverse
249 holds for the subsequent summer period starting in early June, pointing to earlier and more rapid water uptake of the winter
250 crops. In July and August, the approximately constant level of the blue curve indicates that only summer crops continue to
251 consume water while winter crops are in their ripening phase and eventually harvested.

252 Lupine and sunflower were the summer crops which were sown first (March 30, 2021, and April 2, 2021, respectively). Maize
253 was sown on April 16, 2021, and soy on May 15, 2021. The loadings of lupine, which were rather performing like winter crops
254 than summer crops, indicated that lupine showed an early onset of intensive evapotranspiration, compared to other summer
255 crops, especially sunflower which was sown at the same time.

256 For further investigation of the vegetation effect on PCs, drone imagery taken at the end of May, when sowing has been
257 completed in all patches, and imagery taken at the beginning of July, when winter crops are in the ripening phase, was analysed.
258 The second PC's loadings of the time series from different sensors were compared to the Normalized Difference Vegetation
259 Index (NDVI; available for three dates) and surface temperature (only available for May 31, 2021) of the respective sensor
260 location as a proxy for actual evapotranspiration. At the end of May, the NDVI, as a proxy for photosynthesis potential, was
261 positively correlated with the loadings (Table 4). Surface temperature exhibited a negative correlation. The spatial pattern of
262 surface temperature is assumed to be inversely related to that of actual evapotranspiration. Thus, both proxies, NDVI and
263 surface temperature, support the inference that in this study positive loadings on this principal component represent sites with
264 above-average plant activity and root water uptake at the end of May. This holds for sensors from all depths but was the closest
265 for 0.9 m depth (Pearson correlation of $r = -0.916$ for surface temperature and of $r = 0.946$ for NDVI on May 31). The results
266 in July compared to those in May support the observation. At the time when the winter crops are already in the ripening phase
267 and the summer crops reach high levels of evapotranspiration, the correlations are being reversed and negative loadings
268 indicate above-average plant activity for summer crops. On July 06, highest Pearson correlations for NDVI are found for 0.6
269 m depth ($r = -0.917$).

270 3.2.3 Third principal component

271 The third PC explained 4.1% of the total data set's variance. Loadings ranged between -0.787 and 0.244 with a median of
272 0.006. Extreme loadings (< -0.25) were found only for sensors in 0.9 m depth in patches 66, 89, 95 and 102 (Figure 6). The
273 location of these patches shows a certain regionalspatial pattern, with the patches roughly following an east-west direction
274 rather than showing-abeing distributed randomly location-within the field. This may point to topography or soil structure
275 causing deviations from mean soil moisture behaviour for patches located near this gradient. However, this pattern cannot be
276 assigned to topography or structures apparent on the topsoil map (Figure 1). Loadings were closely related to the minima of
277 the z-transformed soil moisture in the period from December to February ($r = 0.70$, $p < 0.001$, Figure 7). What distinguishes
278 the orange line (negative loading on PC3) from the blue line (positive loading on PC3) -is the higher temporal variability and
279 the delayed reaching of maxima in the first half of the study period (Figure 8).

280 **3.2.4 Fourth principal component**

281 The fourth PC explained 2.2% of the total data set's variance. The loadings were clustered by crop groups. All fallow patches
282 showed consistent positive loadings while the patches which were covered by winter crops, showed mainly negative loadings
283 except in patch 95 where the loadings of the two sensors in 0.3 m depth were slightly above zero (Figure 9). According to the
284 Wilcoxon-Mann test treatment group B (fallow, followed by summer crops) differed significantly from group A (winter crops)
285 and C (cover crops, followed by summer crops) whereas there was no significant difference between group A and C. In contrast
286 to crop groups A and B, patches that were covered by the cover crop phacelia during the winter months, did not show one-
287 directional loadings.

288 Figure 10 illustrates the effect of the fourth PC on time series. The blue line (positive loading) shows a hydrological behaviour
289 which -would be typical for more sandy soils -while the orange line (negative loading) depicts behaviour that one would expect
290 in more loamy soils due to its delayed responses to rainstorms and subsequent less steep recovery. The patterns in the loadings
291 thus show a differentiation between patches with winter crops and fallow patches in the winter months (Figure 9). However,
292 it is not clear how winter crops on the one side and fallow on the other side could induce such a different soil water behaviour
293 shown in Figure 10.

294 **3.2.5 Fifth principal component**

295 The fifth PC explained 1.7% of the data set's variance. The loadings showed a depth-related pattern. All time series from the
296 0.3 m depth exhibited negative loadings with two minor exceptions. Whereas all time series from 0.9 m depth showed positive
297 loadings throughout, and time series from 0.6 m depth plot in between. Loadings in 0.6 m depth and 0.9 m depth were mostly
298 more similar to each other than to the loadings of 0.3 m depth (Figure 11). The Pearson correlation coefficient between loadings
299 and depth was $r = 0.710$ ($p < 0.05$). Thus it can be concluded that the fifth PC reflected the effect of soil depth on soil moisture
300 variance. This effect differed between crops, with the three most negative loadings found in maize patches while the three
301 most positive loadings were found in lupine patches. The soil water dynamics show a damping effect with increasing depth
302 (Figure 12) from little damping for sensors in the upper depth (orange line) to higher damping for sensors in greater depth
303 (blue line).

304 Neither patterns in topography nor in weeding management modes were reflected in the loadings of PC1-PC5. Due to the lack
305 of subsurface soil data, no additional findings could be derived from the Geophilus texture analysis.

306 **4 Discussion**

307 A PCA was conducted to identify the drivers of soil moisture variability in a diversified cropping field. Data consisted of
308 observed time series from 64 soil moisture probes. Results showed that the first five principal components described about
309 97% of the variance of the data set, -and revealed various effects of weather, soil texture, soil depth, crops, and management
310 schemes (Table 3). The first principal component captured 72% of the total variance. Consequently, 72% of the observed

311 dynamics could be described by a lumped model that would not consider any within-field heterogeneity. These results are in
312 the range of similar studies. Martini et al. (2017) found that the first PC explained 58% of the variance of a data set that
313 comprised both agricultural fields as well as grassland transects. Similarly, Lischeid et al. (2017) ascribed 70% of the variance
314 of a forest soil moisture data set to a single component. In the study by Hohenbrink et al. (2016), 85% of the variance of soil
315 moisture data in a set of arable field experiments with two different crop rotation schemes was attributed to the first principal
316 component. The strong influence of weather conditions as it is shown in our study is confirmed by Choi et al. (2007) who
317 showed that rainfall, next to topography, explained most of the surface soil moisture variability.

318 **4.1 Crop effects**

319 As Korres et al. (2015) stated that vegetation and management (e.g. planting and harvesting dates) are among the main causes
320 for spatial variability of soil moisture in agricultural fields. In this study, around 17% of the total variance at the field scale
321 was attributed to the vegetation effect. When not considering the temporal component reflected by PC1 and thus only looking
322 at the spatial variability, 61% of the remaining variance is caused by the vegetation effect reflected by PC2. Korres et al. (2010)
323 also used PCA to identify the drivers of spatial variability of soil moisture within a cropped area but did not find such a
324 pronounced vegetation effect. In their study, more than two thirds of the spatial variability was related to soil parameters and
325 topography. In contrast, the strong influence of vegetation in our study may be due to the high level of crop diversification.
326 Within single crop fields, vegetation effects are observable due to heterogeneous biomass or root development (Brown et al.,
327 2021; Korres et al., 2010), but may be of a lower magnitude compared to fragmented field arrangements with different crops.
328 The high impact of crop diversification on soil moisture variability is also visible when comparing our results to the results of
329 a field under comparable conditions in the same region with only two crop rotations in which only 3.8% was explained by the
330 different crop rotations (Hohenbrink et al., 2016). Joshi and Mohanty (2010) also assessed the effect of vegetation in their
331 study in which they investigated spatial soil moisture variability at the field to regional scale in the Southern Great Plains
332 regions in the US by means of PCA and assessed the effect of vegetation—. With none of the first seven PC showing strong
333 correlation with vegetation parameters, n contrast to this study the effect of vegetation was—as limited in contrast to our study.
334 since none of the first seven PC showed strong correlations with vegetation parameters.

335
336 It needs to be considered that the proportion of the vegetation effect on soil moisture variability does not only vary spatially
337 and over depth, but also over time. Under dry conditions, soil-plant interactions prevail while under moist conditions,
338 percolation behaviour is predominant (Baroni et al., 2013). The scores are time series and reflect the effect size of a particular
339 process represented by the respective PC. The more the scores of a certain PC deviate from zero during specific periods, the
340 stronger the respective effect is. Consequently, the time series of PC2 scores indicates that the effect of vegetation on total
341 variability varies by time. In accordance with literature, the absolute values of the scores of PC2, representing differences
342 between the contrasting seasonality of crops, are highest in the dry months, May to August. This is mostly explained by the
343 high water demand of summer crops, which are in their vegetative growth stage from May to August, whereas winter crops

344 are already in their reproductive growth stage, including maturity, senescence and harvest where water uptake by crops is
345 minimal or absent (Zhao et al, 2018). In the moist winter months January to March, as well as during the heavy rainfall event
346 in July, the scores of PC2 are relatively small, showing that spatial variability at that time is caused by other factors.
347 The second principal component clearly differentiated between winter and summer crops, which was driven by the different
348 seasonal patterns of root water uptake (Figure 4). In contrast, the fourth component differentiated between fallow followed by
349 summer crops and winter crops, whereas phacelia followed by summer crop did not show a clear pattern (Figure 9). Phacelia
350 is grown as a cover crop and usually dies off in frost periods. Due to rather mild winter temperatures 2020/21, Phacelia was
351 not terminated efficiently and kept growing until spring, until it was terminated mechanically. It was recently shown that the
352 timing of removal of winter cover crops is key to provide soil water recharge for the subsequent crop, as the depletion of soil
353 water in autumn is significant (Selzer and Schubert, 2023). Thus, some Phacelia patches exhibited negative loadings, similarly
354 to the winter crop patches, while other patches with most likely different termination dates exhibited positive loadings.
355 Hence, the fourth component obviously reflected the effect of the active root system in the winter period. According to this
356 component, soil water dynamics in the fallow patches mostly resembled the typical behaviour expected for sandy soils, and
357 winter crop patches showed a more damped behaviour that is usually observed in more loamy soils. Note that the term “fallow”
358 refers to crop cover in autumn and winter only. Acharya et al. (2019) found that winter cover crops improved/increased soil
359 moisture from 3% to 5% in the top 0.3 m soil layer which is in line with the findings from of Figure 10 that shows a higher
360 water holding capacity for winter crops (orange line) in winter. However, it has also been observed that roots from winter
361 crops can increase soil porosity and therefore, water mobility in the soil (Lange et al., 2013; Scholl et al., 2014).
362 The delay of percolating water in winter crop and some cover crop patches may also be caused by higher organic matter content
363 in the top soil provided by cover crop roots and crop residues. Further soil-vegetation interactions might play a role for the
364 delayed seepage fluxes of winter crop and part of cover crop patches, such as soil organic matter from cover crops and plant
365 residues (Manns et al., 2014; Koudahe et al., 2022; Rossini et al., 2021). Usually, such effects are assumed to occur only at
366 larger time scales, which is closely related to problems of detecting changes soil organic carbon (SOC) quantity or quality. So
367 far, there is only anecdotal evidence for rather short-term SOC quality affecting soil hydraulic properties even at smaller time
368 scales. Although this effect constituted only a minor share of soil moisture variance (Table 3), it was clearly discernible as a
369 separate principal component. This effect would be worth to be tested in more detailed future studies.

370 **4.2 Soil texture and soil depth effects**

371 Loadings on the third principal component were not related to crop types. In contrast, a spatial pattern emerged: Only sensors
372 from 0.9 m depth from six adjacent patches exhibited strongly negative loadings (Figure 6), whereas all other sensors showed
373 minor positive or negative loadings. This points to an effect of subsoil substrates, that is, higher clay content and consequently
374 higher water holding capacity. That would be consistent with delayed response to seepage fluxes and reduced desiccation in
375 the vegetation period (Figure 8). The strong relation between z-transformed soil moisture minima at the beginning of the study
376 period (Figure 7) which might originate from a delayed response to a prior rainfall, and the regional pattern of the location of

377 the patches following a west-east direction within the experiment might be an indicator of underlying soil structures causing
378 this effect. Data on texture at soil moisture sensor locations in deeper layers would be of high value to confirm the assumptions.
379 Whereas the third principal component seems to reflect a local peculiarity, the fifth component obviously grasps a more generic
380 feature. Loadings on this component are clearly related with depth (Figure 11). Strong positive loadings indicate a strongly
381 damped behaviour of soil moisture time series: The blue line, representing sites with positive loadings on PC5 which is typical
382 for sensors at greater depth (Figure 12), exhibits clearly reduced amplitudes compared to the orange line, that is, sensors at
383 shallow depth. Hohenbrink and Lischeid (2015) combined a hydrological model and principal component analysis to study the
384 effect of soil depth and soil texture on damping of the input signal in more detail. A subsequent field study proved the relevance
385 of that effect in a real-world setting (Hohenbrink et al., 2016). Moreover, Thomas et al. (2012) found that damping accounted
386 for a large share of variance in a set of hydrographs from a region of 30,000 km². Damping was also the most relevant driver
387 of spatial variance in a set of time series of groundwater head at about the same scale (Lischeid et al., 2021).

388 **4.3 Limitations**

389 Data gaps during the studied period occurred due to multiple technical and environmental factors. Data gaps in soil moisture
390 time series were caused by repeated temporary failure of the WSN. There was a failure of one sensor that was replaced and
391 one LoRa node was damaged by intruding water. More relevant, however, were failures of data transmission. Yildiz et al.
392 (2015) point to the problem of optimizing transmission power for data and acknowledgement packets depending on energy
393 dissipation under the given conditions. E.g., saturated soil conditions and dense biomass stands reduce the transmission signal
394 from the node to the gateway (Bogena et al., 2009). The installation of a second gateway in September 2021 increased higher
395 transmission coverage in the field. Another obstacle was snow cover on the gateways' solar panels. Finally, solar panels were
396 subject to theft. However, higher level of maintenance and supervision helped to reduce the number and the length of data
397 gaps.

398 PCA requires gapless time series. Gaps in single time series need to be either filled at the risk of introducing artefacts or the
399 respective time period cannot be considered at all for analysis. This can be seen as a weakness of PCA. On the other hand, and
400 in contrast to other time series analysis approaches, the time series need not to be equidistant. Assigning PCs to processes and
401 effects is not straightforward and might be subject for debate. For example, in this study soil samples were taken at least at 0.8
402 m distance from the sensors to avoid disturbance of the measurements. Due to pronounced small-scale soil variability, these
403 samples are not fully representative for the measurement sites. In spite of these limitations, the PCA results clearly point to
404 various effects worth to be studied in more detail in subsequent studies.

405 **5 Conclusion**

406 The use of PCA has a high value for the application in environmental sciences, as it contributes to process understanding of
407 soil water dynamics by disentangling the different effects of complex spatially and temporally diversified cropping systems.

408 In this study, more than 97% of the observed spatial and temporal variance was assigned to five different effects.
409 Meteorological drivers explained 72.3% of the total variance (PC1). Different seasonal patterns of root water uptake of winter
410 crops compared to summer crops accounted for another 17.0% of variance (PC2). An additional share of 2.2% of variance
411 seemed to be related to the effects of different vegetation cover and its interplay with soil hydraulic properties (PC4).
412 Heterogeneity of subsoil substrates explained 4.1 % of variance (PC3), and the damping effect of input signals over depth
413 another 1.7% (PC5). To summarize, plant-related direct and indirect effects accounted for 19.2% of the variance (PC2 and
414 PC4), and soil-related effects only for 5.8% (PC3 and PC5). In particular, the plant-induced effects on soil hydraulic properties
415 would be worthwhile to be studied in more detail.
416 Findings of this study highly depend on local conditions. However, the methodology itself is generally applicable to other site
417 conditions and can lead to improved management practices through improved knowledge about soil water dynamics.
418 Furthermore, information from this study can also help to develop both parsimonious and tailored mechanistic models for
419 model upscaling. In this regard, principal component analysis of large soil moisture data sets from real-world monitoring setups
420 performed a meaningful diagnostic tool for complex cropping systems.

421 **Acknowledgments**

422 The maintenance of the patchCROP experimental infrastructure and the LoRaWAN soil sensor system is ensured by the
423 Leibniz Centre for Agricultural Landscape Research. The authors acknowledge the additional support from the German
424 Research Foundation under Germany's Excellence Strategy, EXC-2070 – 390732324 – PhenoRob for patchCROP related
425 research activities.

426 The authors thank Gerhard Kast, Thomas von Oepen, Lars Richter, Robert Zieciak, Sigrid Ehlert and Motaz Abdelaziz for
427 their dedicated support in maintenance of the monitoring system and data collection.

428 **Competing interests**

429 The authors declare that they have no conflict of interest.

430 **References**

- 431 Acclima Inc.: True TDR310H. Soil-Water-Temperature-BEC-Sensor, 2019.
- 432 Acharya, B. S., Dodla, S., Gaston, L. A., Darapuneni, M., Wang, J. J., Sepat, S., and Bohara, H.: Winter cover crops effect on
433 soil moisture and soybean growth and yield under different tillage systems, *Soil and Tillage Research*, 195,
434 <https://doi.org/10.1016/j.still.2019.104430>, 2019.

435 Alhameid, A., Singh, J., Sekaran, U., Ozlu, E., Kumar, S., and Singh, S.: Crop rotational diversity impacts soil physical and
436 hydrological properties under long-term no- and conventional-till soils, *Soil Res.*, 58, 84, <https://doi.org/10.1071/SR18192>,
437 2020.

438 Baroni, G., Ortuani, B., Facchi, A., and Gandolfi, C.: The role of vegetation and soil properties on the spatio-temporal
439 variability of the surface soil moisture in a maize-cropped field, *Journal of Hydrology*, 489, 148–159,
440 <https://doi.org/10.1016/j.jhydrol.2013.03.007>, 2013.

441 BIRTHAL, P. S. and Hazrana, J.: Crop diversification and resilience of agriculture to climatic shocks: Evidence from India,
442 *Agricultural Systems*, 173, 345–354, <https://doi.org/10.1016/j.agsy.2019.03.005>, 2019.

443 Bogena, H. R., Huisman, J. A., Meier, H., and Weuthen, A.: Hybrid wireless underground sensor networks: Quantification of
444 signal attenuation in soil, *Vadose Zone J.*, 8, 755-761, <https://doi.org/10.2136/vzj2008.0138>, 2009.

445 Bogena, H. R., Weuthen, A., and Huisman, J. H.: Recent Developments in Wireless Soil Moisture Sensing to Support Scientific
446 Research and Agricultural Management, *Sensors*, 22, 9792, <https://doi.org/10.3390/s22249792>, 2022.

447 Bönecke, E., Meyer, S., Vogel, S., Schröter, I., Gebbers, R., Kling, C., Kramer, E., Lück, K., Nagel, A., Philipp, G., Gerlach,
448 F., Palme, S., Scheibe, D., Zieger, K., Rühlmann, J.: Guidelines for precise lime management based on high-resolution soil
449 pH, texture and SOM maps generated from proximal soil sensing data, *Precision Agric*, 22, 493-523,
450 <https://doi.org/10.1007/s11119-020-09766-8>, 2021.

451 Bretherton, C. S., Smith, C., and Wallace, J. M.: An intercomparison of methods for finding coupled patterns in climate data,
452 *Journal of Climatology*, 5, 541–560, 1992.

453 Brocca, L., Melone, F., Moramarco, T., and Morbidelli, R.: Spatial-temporal variability of soil moisture and its estimation
454 across scales, *Water Resour. Res.*, 46, <https://doi.org/10.1029/2009WR008016>, 2010.

455 Brown, M., Heinse, R., Johnson-Maynard, J., and Huggins, D.: Time-lapse mapping of crop and tillage interactions with soil
456 water using electromagnetic induction, *Vadose zone j.*, 20, <https://doi.org/10.1002/vzj2.20097>, 2021.

457 Cardell-Oliver, R., Hübner, C., Leopold, M., and Beringer, J.: Dataset: LoRa Underground Farm Sensor Network, in:
458 *Proceedings of the 2nd Workshop on Data Acquisition To Analysis - DATA '19*, the 2nd Workshop, New York, NY, USA,
459 26–28, <https://doi.org/10.1145/3359427.3361912>, 2019.

460 Choi, M., Jacobs, J. M., and Cosh, M. H.: Scaled spatial variability of soil moisture fields, *Geophys. Res. Lett.*, 34,
461 <https://dx.doi.org/10.1029/2006GL028247>, 2007.

462 Deumlich, D., Ellerbrock, R. H., and Frielinghaus, Mo.: Estimating carbon stocks in young moraine soils affected by erosion,
463 *CATENA*, 162, 51–60, <https://doi.org/10.1016/j.catena.2017.11.016>, 2018.

464 Donat, M., Geistert, J., Grahmann, K., Bloch, R., and Bellingrath-Kimura, S. D.: Patch cropping- a new methodological
465 approach to determine new field arrangements that increase the multifunctionality of agricultural landscapes, *Computers and*
466 *Electronics in Agriculture*, 197, 106894, <https://doi.org/10.1016/j.compag.2022.106894>, 2022.

467 DIN ISO 11277: Soil quality - Determination of particle size distribution in mineral soil material - Method by sieving and
468 sedimentation (ISO 11277:1998 + ISO 11277:1998 Corrigendum 1:2002), Beuth-Verlag, Berlin,
469 <https://dx.doi.org/10.31030/9283499>, 2002.

470 DWD Climate Data Center (CDC): Historische tägliche Stationsbeobachtungen (Temperatur, Druck, Niederschlag,
471 Sonnenscheindauer, etc.) für Deutschland, Version v21.3, 2021.

- 472 Fischer, C., Roscher, C., Jensen, B., Eisenhauer, N., Baade, J., Attinger, S., Scheu, S., Weisser, W. W., Schumacher, J.,
473 Hildebrandt, A.: How Do Earthworms, Soil Texture and Plant Composition Affect Infiltration along an Experimental Plant
474 Diversity Gradient in Grassland?, PLoS ONE, 9, 6, <https://doi.org/10.1371/journal.pone.0098987>, 2014.
- 475 Fischer, G. F., Nachtergaele, S., Prieler, S., van Velthuisen, H. T., Verelst, L., and Wisberg, D.: Global Agro-ecological Zones
476 Assessment for Agriculture (GAEZ 2008), IIASA, Laxenburg, Austria and FAO, Rome, 2008.
- 477 GeoBasis-DE and Landesvermessung und Geobasisinformation Brandenburg (LGB): Digitales Geländemodell (DGM),
478 Landesvermessung und Geobasisinformation Brandenburg (LGB), Potsdam, 2021.
- 479 Graf, A., Bogena, H. R., Drüe, C., Herdelauf, H., Pütz, T., Heinemann, G., and Vereecken, H.: Spatiotemporal relations
480 between water budget components and soil water content in a forested tributary catchment, Water Resour. Res., 50, 4837-
481 4857, <https://doi.org/10.1002/2013WR014516>, 2014.
- 482 Grahmann, K., Reckling, M., Hernandez-Ochoa, I., and Ewert, F.: An agricultural diversification trial by patchy field
483 arrangements at the landscape level: The landscape living lab “patchCROP,” in: Aspects of Applied Biology, Intercropping
484 for sustainability: Research developments and their application, 385–391, 2021.
- 485 Hohenbrink, T. L. and Lischeid, G.: Does textural heterogeneity matter? Quantifying transformation of hydrological signals
486 in soils, Journal of Hydrology, 523, 725–738, <https://doi.org/10.1016/j.jhydrol.2015.02.009>, 2015.
- 487 Hohenbrink, T. L., Lischeid, G., Schindler, U., and Hufnagel, J.: Disentangling the Effects of Land Management and Soil
488 Heterogeneity on Soil Moisture Dynamics, Vadose Zone Journal, 15, <https://doi.org/10.2136/vzj2015.07.0107>, 2016.
- 489 Hupet, F. and Vanclooster, M.: Intraseasonal dynamics of soil moisture variability within a small agricultural maize cropped
490 field, Journal of Hydrology, 261, 86–101, 2002.
- 491 IUSS Working Group WRB: World Reference Base for Soil Resources 2014, Update 2015, International Soil Classification
492 System for Naming Soils and Creating Legends for Soil Maps, World Soil Resources Reports No. 106, Rome: FAO, 2015.
- 493 Jolliffe, I. T.: Principal component analysis. Springer Series in Statistics, Springer, New York, 2002.
- 494 Joshi, C. and Mohanty, B. P.: Physical controls of near-surface soil moisture across varying spatial scales in an agricultural
495 landscape during SMEX02: Physical controls of soil moisture, Water Resour. Res., 46,
496 <https://doi.org/10.1029/2010WR009152>, 2010.
- 497 Kaiser, H. F.: The Application of Electronic Computers to Factor Analysis, Educ.Psychol. Measur., 20,
498 <https://doi.org/10.1177/001316446002000116>, 1960.
- 499 Karlen, D. L., Hurley, E. G., Andrews, S. S., Cambardella, C. A., Meek, D. W., Duffy, M. D., and Mallarino, A. P.: Crop
500 Rotation Effects on Soil Quality at Three Northern Corn/Soybean Belt Locations, Agron.j., 98, 484–495,
501 <https://doi.org/10.2134/agronj2005.0098>, 2006.
- 502 Khan, H., Farooque, A. A., Acharya, B., Abbas, F., Esau, T. J., and Zaman, Q. U.: Delineation of Management Zones for Site-
503 Specific Information about Soil Fertility Characteristics through Proximal Sensing of Potato Fields, Agronomy, 10, 1854,
504 <https://doi.org/10.3390/agronomy10121854>, 2020.
- 505 Korres, W., Koyama, C. N., Fiener, P., and Schneider, K.: Analysis of surface soil moisture patterns in agricultural landscapes
506 using Empirical Orthogonal Functions, Hydrol. Earth Syst. Sci., 14, 751–764, <https://doi.org/10.5194/hess-14-751-2010>, 2010.

- 507 Korres, W., Reichenau, T. G., Fiener, P., Koyama, C. N., Bogen, H. R., Cornelissen, T., Baatz, R., Herbst, M., Diekkrüger,
508 B., Vereecken, H., and Schneider, K.: Spatio-temporal soil moisture patterns – A meta-analysis using plot to catchment scale
509 data, *Journal of Hydrology*, 520, 326–341, <https://doi.org/10.1016/j.jhydrol.2014.11.042>, 2015.
- 510 Koudahe, K., Allen, S. C., Djaman, K.: Critical review of the impact of cover crops on soil properties, *International Soil and*
511 *Water Conservation Research*, 10, 343–354, <https://doi.org/10.1016/j.iswcr.2022.03.003>, 2022.
- 512 Krauss, L., Hauck, C., and Kottmeier, C.: Spatio-temporal soil moisture variability in Southwest Germany observed with a
513 new monitoring network within the COPS domain, *metz*, 19, 523–537, <https://doi.org/10.1127/0941-2948/2010/0486>, 2010.
- 514 Lange, B., Germann, P. F., and Lüscher, P.: Greater abundance of *Fagus sylvatica* in coniferous flood protection forests due
515 to climate change: impact of modified root densities on infiltration, *Eur J Forest Res*, 132, 151–163,
516 <https://doi.org/10.1007/s10342-012-0664-z>, 2013.
- 517 Lehr, C. and Lischeid, G.: Efficient screening of groundwater head monitoring data for anthropogenic effects and measurement
518 errors, *Hydrol. Earth Syst. Sci.*, 24, 501–513, <https://doi.org/10.5194/hess-24-501-2020>, 2020.
- 519 Lischeid, G., Frei, S., Huwe, B., Bogner, C., Lüers, J., Babel, W., and Foken, T.: Catchment Evapotranspiration and Runoff,
520 in: *Energy and Matter Fluxes of a Spruce Forest Ecosystem*, vol. 229, Springer, Cham, Cham, 355–375, 2017.
- 521 Lischeid, G., Dannowski, R., Kaiser, K., Nützmann, G., Steidl, J., and Stüve, P.: Inconsistent hydrological trends do not
522 necessarily imply spatially heterogeneous drivers, *Journal of Hydrology*, 596, 126096,
523 <https://doi.org/10.1016/j.jhydrol.2021.126096>, 2021.
- 524 Lloret, J., Sendra, S., Garcia, L., and Jimenez, J. M.: A Wireless Sensor Network Deployment for Soil Moisture Monitoring
525 in Precision Agriculture, *Sensors*, 21, 7243, <https://doi.org/10.3390/s21217243>, 2021.
- 526 Lueck, E. and Ruehlmann, J.: Resistivity mapping with *Geophilus Electricus* - Information about lateral and vertical soil
527 heterogeneity, *Geoderma*, 199, 2–11, <https://doi.org/10.1016/j.geoderma.2012.11.009>, 2013.
- 528 Mahmood, R., Littell, A., Hubbard, K. G., and You, J.: Observed data-based assessment of relationships among soil moisture
529 at various depths, precipitation, and temperature, *Applied Geography*, 34, 255–264,
530 <https://doi.org/10.1016/j.apgeog.2011.11.009>, 2012.
- ~~531 Manns, H. R., Berg, A. A., Bullock, P. R., & McNairn, H.: Impact of soil surface characteristics on soil water content variability
532 in agricultural fields: Field scale soil water content variability. *Hydrological Processes*, 28, 14, 4340–4351,
533 <https://doi.org/10.1002/hyp.10216>, 2014.~~
- 534 Martini, E., Wollschläger, U., Musolff, A., Werban, U., and Zacharias, S.: Principal Component Analysis of the Spatiotemporal
535 Pattern of Soil Moisture and Apparent Electrical Conductivity, *Vadose Zone J*, 16, vjz2016.12.0129,
536 <https://doi.org/10.2136/vzj2016.12.0129>, 2017.
- 537 Nied, M., Hundecha, Y., and Merz, B.: Flood-initiating catchment conditions: a spatio-temporal analysis of large-scale soil
538 moisture patterns in the Elbe River basin, *Hydrol. Earth Syst. Sci.*, 17, 1401–1414, <https://doi.org/10.5194/hess-17-1401-2013>,
539 2013.
- 540 Nunes, M. R., van Es, H. M., Schindelbeck, R., Ristow, A. J., Ryan, M.: No-till and cropping system diversification improve
541 soil health and crop yield, *Geoderma*, 328, 30–43, <https://doi.org/10.1016/j.geoderma.2018.04.031>, 2018.
- 542 Pan, F. and Peters-Lidard, C. D.: On the Relationship Between Mean and Variance of Soil Moisture Fields, *JAWRA Journal*
543 *of the American Water Resources Association*, 44, 235–242, <https://doi.org/10.1111/j.1752-1688.2007.00150.x>, 2008.

- 544 Paroda, Raj. S., Suleimenov, M., Yusupov, H., Kireyev, A., Medeubayev, R., Martynova, L., and Yusupov, K.: Crop
545 Diversification for Dryland Agriculture in Central Asia, in: *CSSA Special Publications*, edited by: Rao, S. C. and Ryan, J.,
546 Crop Science Society of America and American Society of Agronomy, Madison, WI, USA, 139–150,
547 <https://doi.org/10.2135/cssaspecpub32.c9>, 2015.
- 548 Placidi, P., Morbidelli, R., Fortunati, D., Papini, N., Gobbi, F., and Scorzoni, A.: Monitoring Soil and Ambient Parameters in
549 the IoT Precision Agriculture Scenario: An Original Modeling Approach Dedicated to Low-Cost Soil Water Content Sensors,
550 *Sensors*, 21, 5110, <https://doi.org/10.3390/s21155110>, 2021.
- 551 Prakosa, S. W., Faisal, M., Adhitya, Y., Leu, J.-S., Köppen, M., and Avian, C.: Design and Implementation of LoRa Based
552 IoT Scheme for Indonesian Rural Area, *Electronics*, 10, 77, <https://doi.org/10.3390/electronics10010077>, 2021.
- 553 R Development Core Team: R: A Language and Environment for Statistical Computing, R Foundation for Statistical
554 Computing (Version 4.1.0, <http://www.R-project.org>), Vienna, 2021.
- 555 Rodriguez, C., Mårtensson, L.-M. D., Jensen, E. S., and Carlsson, G.: Combining crop diversification practices can benefit
556 cereal production in temperate climates, *Agron. Sustain. Dev.*, 41, 48, <https://doi.org/10.1007/s13593-021-00703-1>, 2021.
- 557 Rossini, P. R., Ciampitti, I. A., Hefley, T., and Patrignani, A.: A soil moisture-based framework for guiding the number and
558 location of soil moisture sensors in agricultural fields, *Vadose zone J.*, 20, <https://doi.org/10.1002/vzj2.20159>, 2021.
- 559 Salam, A.: *Internet of Things for Sustainable Community Development: Wireless Communications, Sensing, and Systems*,
560 Springer International Publishing, Cham, Switzerland, <https://doi.org/10.1007/978-3-030-35291-2>, 2020.
- 561 Salam, A. and Raza, U.: *Signals in the Soil: Developments in Internet of Underground Things*, Springer International
562 Publishing, Cham, Switzerland, <https://doi.org/10.1007/978-3-030-50861-6>, 2020.
- 563 Scheffer, F. and Schachtschabel, P.: *Lehrbuch der Bodenkunde*, 15th ed., Spektrum Akademischer Verlag GmbH. Berlin,
564 Heidelberg, <https://doi.org/10.1007/978-3-662-55871-3>, 2002.
- 565 Scholl, P., Leitner, D., Kammerer, G., Loiskandl, W., Kaul, H.-P., and Bodner, G.: Root induced changes of effective 1D
566 hydraulic properties in a soil column, *Plant Soil*, 381, 193–213, <https://doi.org/10.1007/s11104-014-2121-x>, 2014.
- 567 Selzer, T., and Schubert, S.: Water dynamics of cover crops: No evidence for relevant water input through occult precipitation,
568 *J Agro Crop Sci.*, 209, 422–437, <https://doi.org/10.1111/jac.12631>, 2023.
- 569 Si, B. C.: Spatial Scaling Analyses of Soil Physical Properties: A Review of Spectral and Wavelet Methods, *Vadose Zone*
570 *Journal*, 7, 547–562, <https://doi.org/10.2136/vzj2007.0040>, 2008.
- 571 Sponagel, H., Grottenthaler, W., Hartmann, K.J., Hartwich, R., Janetzko, P., Joisten, H., Kühn, D., Sabel, K.J., Traidl, R.
572 (Eds.): *Bodenkundliche Kartieranleitung (German Manual of Soil Mapping, KA5)*, 5th edition, Bundesanstalt für
573 Geowissenschaften und Rohstoffe, Hannover, 2005.
- 574 Strebelle, S., Payrazyan, K., and Caers, J.: Modeling of a Deepwater Turbidite Reservoir Conditional to Seismic Data Using
575 Principal Component Analysis and Multiple-Point Geostatistics, *SPE Journal*, 8, 227–235, <https://doi.org/10.2118/85962-PA>,
576 2003.
- 577 Tamburini, G., Bommarco, R., Wanger, T. C., Kremen, C., van der Heijden, M. G. A., Liebman, M., and Hallin, S.:
578 Agricultural diversification promotes multiple ecosystem services without compromising yield, *Sci. Adv.*, 6, eaba1715,
579 <https://doi.org/10.1126/sciadv.aba1715>, 2020.
- 580 Taylor, J. and Whelan, B.: *A General Introduction to Precision Agriculture*, 2010.

- 581 Thomas, B., Lischeid, G., Steidl, J., and Dannowski, R.: Regional catchment classification with respect to low flow risk in a
582 Pleistocene landscape, *Journal of Hydrology*, 475, 392–402, <https://doi.org/10.1016/j.jhydrol.2012.10.020>, 2012.
- 583 Trnka, M., Rötter, R. P., Ruiz-Ramos, M., Kersebaum, K. C., Olesen, J. E., Žalud, Z., and Semenov, M. A.: Adverse weather
584 conditions for European wheat production will become more frequent with climate change, *Nature Clim Change*, 4, 637–643,
585 <https://doi.org/10.1038/nclimate2242>, 2014.
- 586 Vachaud, G., Passerat De Silans, A., Balabanis, P., Vauclin, M.: Temporal Stability of Spatially Measured Soil Water
587 Probability Density Function, *Soil Science Society of America Journal*, 49, 822-828,
588 <https://doi.org/10.2136/sssaj1985.03615995004900040006x>, 1985.
- 589 Vanderlinden, K., Vereecken, H., Hardelauf, H., Herbst, M., Martínez, G., Cosh, M. H., Pachepsky, Y. A.: Temporal Stability
590 of Soil Water Contents: A Review of Data and Analyses, *Vadose Zone J.*, <https://doi.org/10.2136/vzj2011.0178>, 2012.
- 591 Vereecken, H., Huisman, J. A., Pachepsky, Y., Montzka, C., van der Kruk, J., Bogaen, H., Weihermüller, L., Herbst, M.,
592 Martínez, G., and Vanderborght, J.: On the spatio-temporal dynamics of soil moisture at the field scale, *Journal of Hydrology*,
593 516, 76–96, <https://doi.org/10.1016/j.jhydrol.2013.11.061>, 2014.
- 594 Yildiz, H. U., Tavli, B., and Yanikomeroglu, H.: Transmission power control for link-level handshaking in wireless sensor
595 networks, *IEEE Sensors Journal*, 16, 2, 561-576. 2015.
- 596 Zhao, X., Li, F., Ai, Z., Li, J., and Gu, C.: Stable isotope evidences for identifying crop water uptake in a typical winter wheat–
597 summer maize rotation field in the North China Plain, *Science of The Total Environment*, 618, 121-131,
598 <https://doi.org/10.1016/j.scitotenv.2017.10.315>, 2018.
- 599 Zhao, Y., Peth, S., Wang, X. Y., Lin, H., and Horn, R.: Controls of surface soil moisture spatial patterns and their temporal
600 stability in a semi-arid steppe, *Hydrol. Process.*, 24, 2507–2519, <https://doi.org/10.1002/hyp.7665>, 2010.

601 Figures and Tables

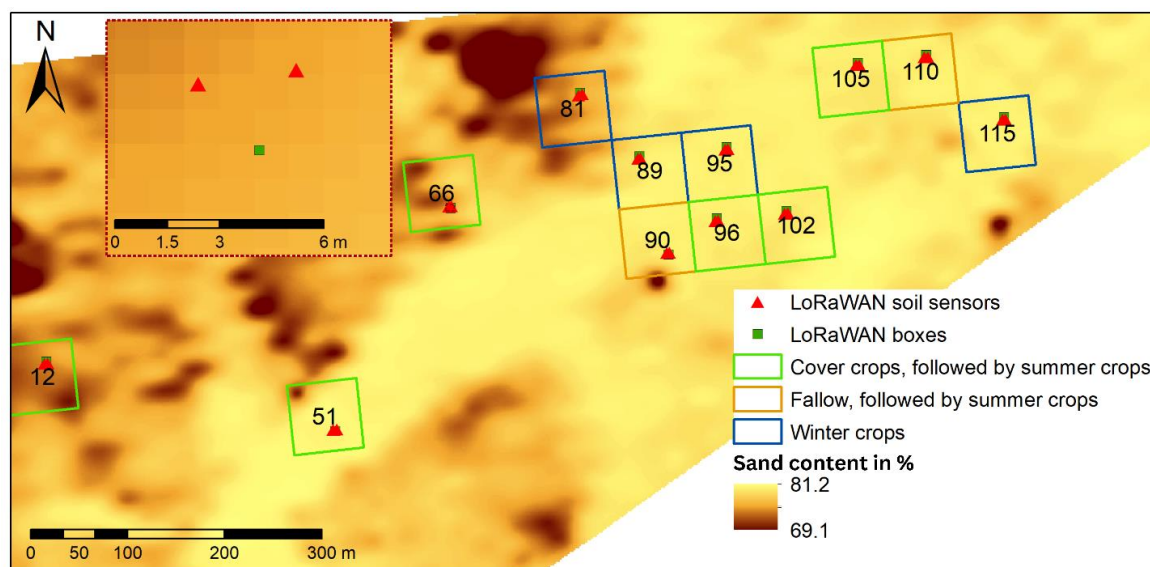
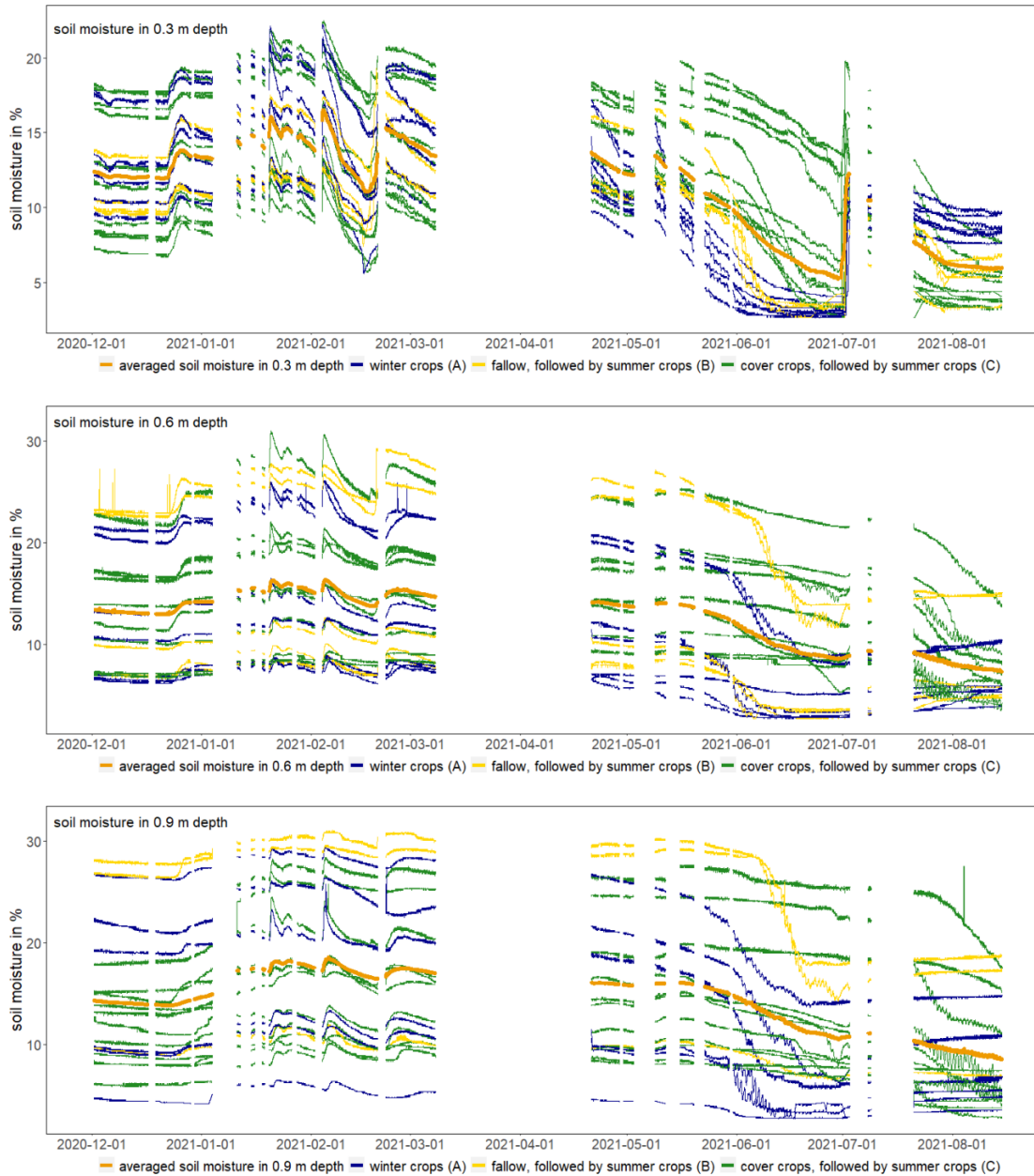
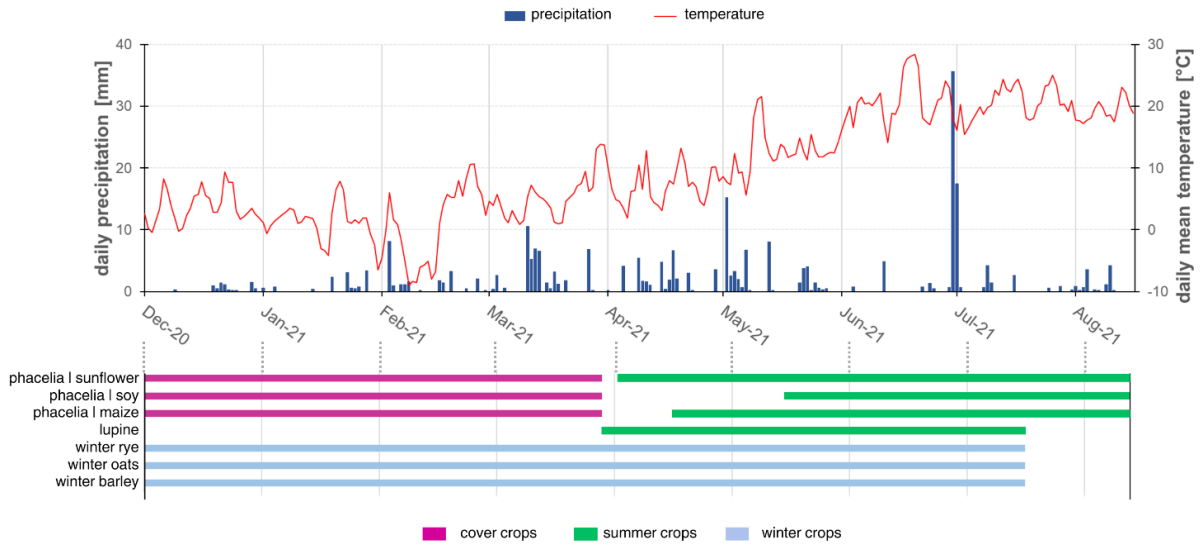


Figure 1: Sand content in % in the top 0.25 m soil depth, -location of the analysed patches, soil sensors (triangle) and boxes (square) under different crop rotations at the patchCROP landscape laboratory experiment, Tempelberg, Brandenburg, Germany.



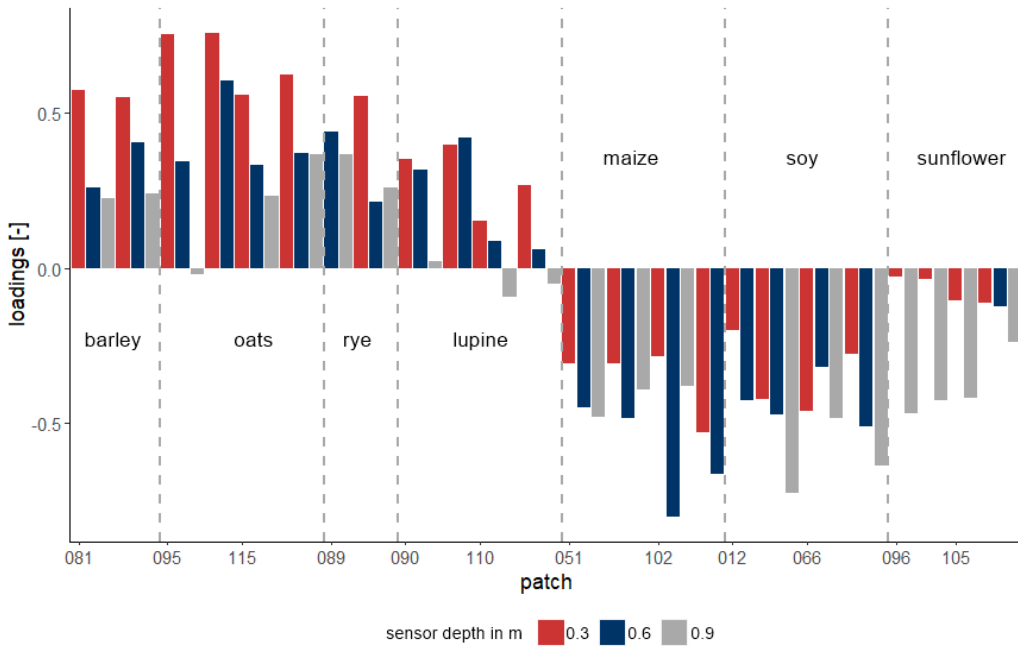
606

607 **Figure 2: Input soil moisture time series per depth, differentiated between crop groups, and average soil moisture of all time series**
 608 **per depth from 2020-12-01 until 2021-08-15 at the patchCROP landscape laboratory experiment, Tempelberg, Brandenburg,**
 609 **Germany.**



610

611 **Figure 3: Measured daily precipitation, mean temperature and cultivated crops - differentiated between winter crops (light blue**
 612 **bars), summer crops (green bars) and cover crops (pink bars) - from 2020-12-01 until 2021-08-15 at the patchCROP landscape**
 613 **laboratory experiment, Tempelberg, Brandenburg, Germany. Specific crops for the studied timeframe stated at the left side of the**
 614 **horizontal bars.**

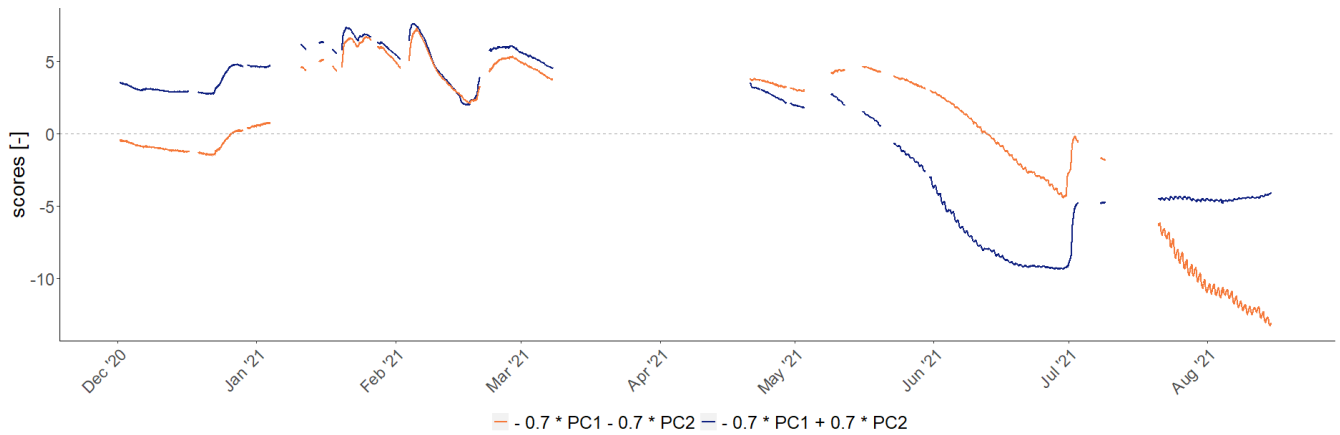


615

616

617 **Figure 4: Time series loadings on the second principal component at the patchCROP landscape laboratory experiment,**
 618 **Tempelberg, Brandenburg, Germany, showing a crop group related pattern. Bars represent individual time series grouped by**
 619 **patch ID and sorted by crop.**

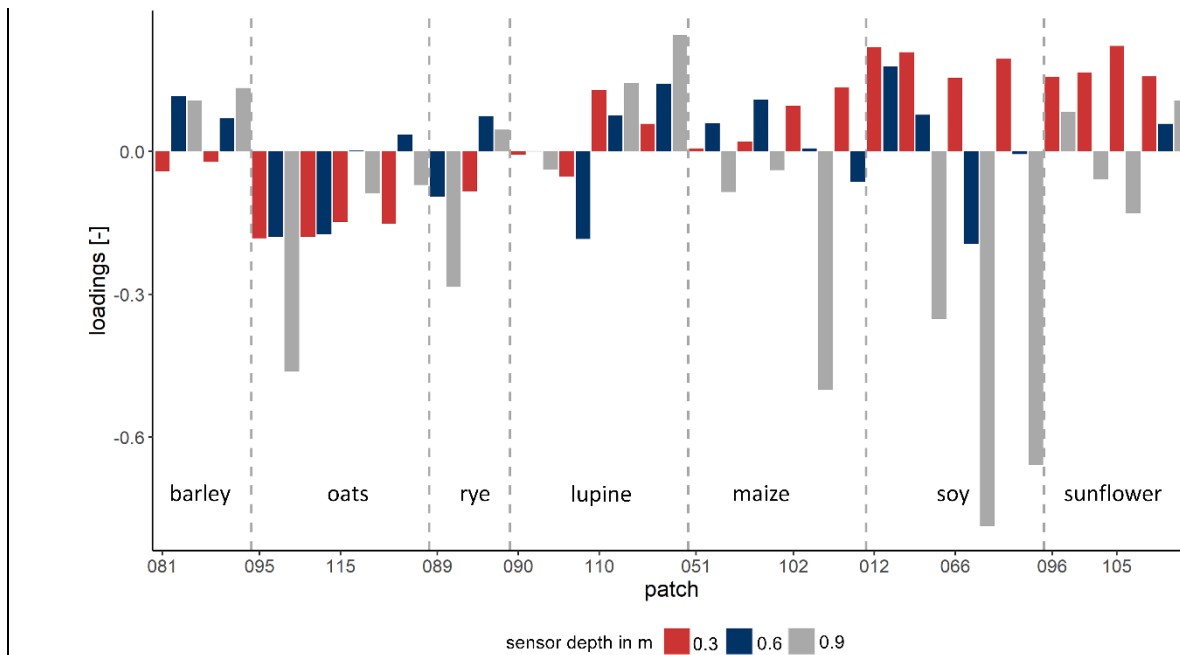
620



621

622 **Figure 5: Effect of the second principal component on modification of the general mean behaviour presented by the first principal**
 623 **component_ at the patchCROP landscape laboratoryexperiment, Tempelberg.** The blue line represents deviations from mean soil
 624 **moisture for time series with positive loadings on PC2 (winter crops) while the orange line represents deviations from mean soil**
 625 **moisture for time series with negative loadings on PC2 (summer crops).**

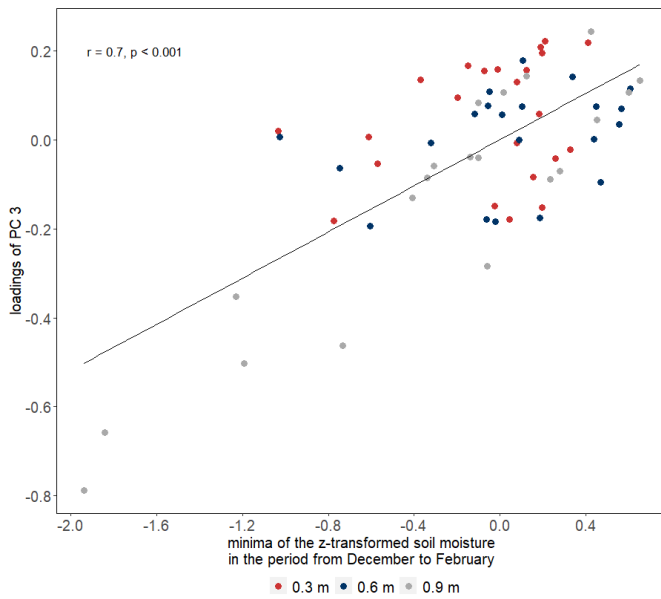
626



627

628

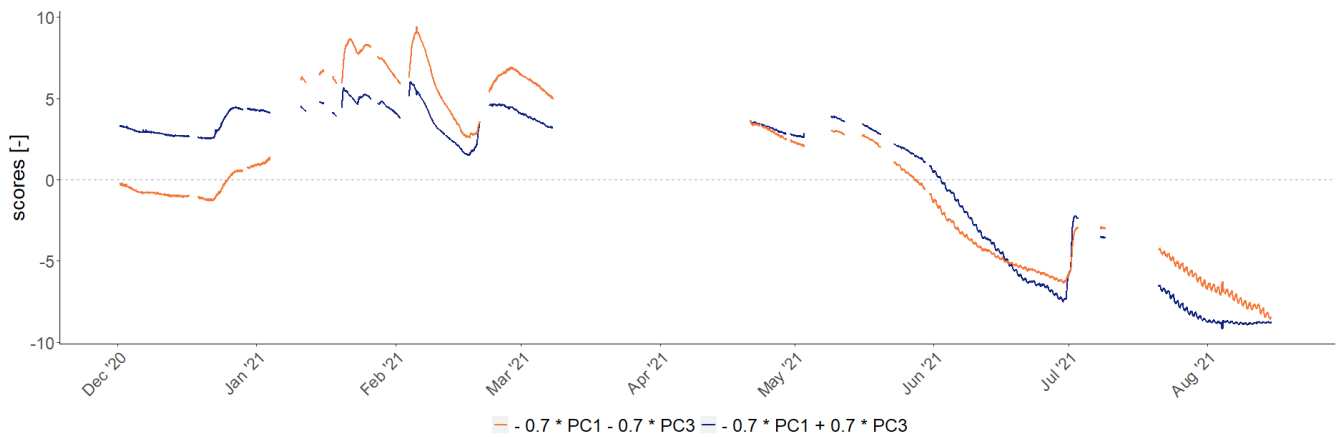
629 **Figure 6: Loadings of time series on the third principal component at the patchCROP landscape laboratoryexperiment,**
 630 **Tempelberg, Brandenburg, Germany with some of the sensors in deeper layers showing noticeably negative loadings. Bars**
 631 **represent individual time series grouped by patch ID and sorted by crop.**



632

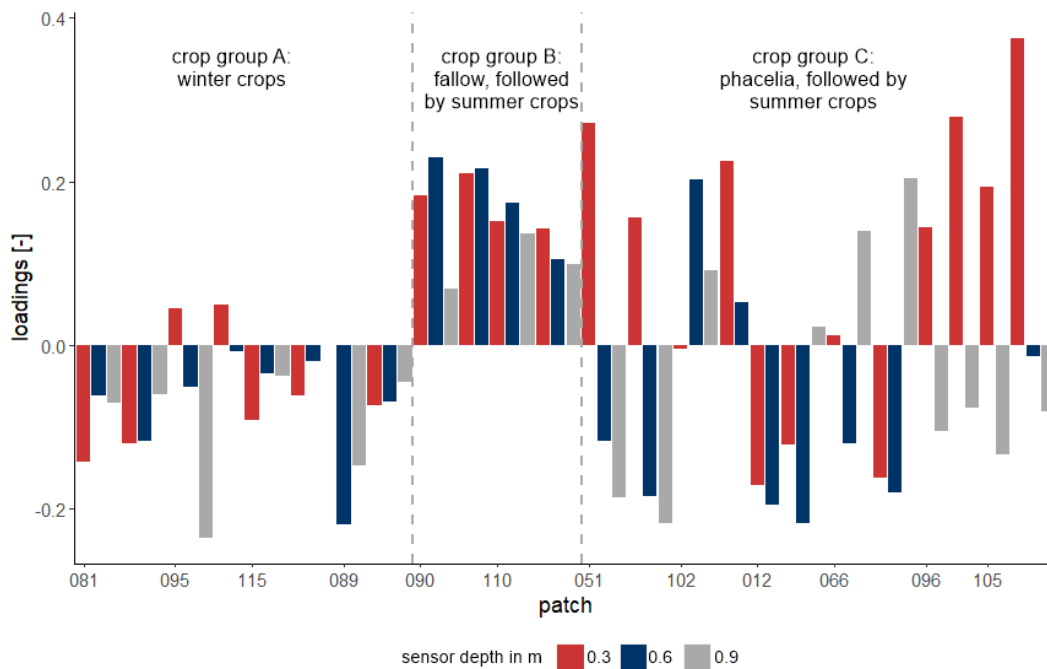
633 **Figure 7: Relation between minima of the z-transformed soil moisture in the first months of the study period with loadings of third**
 634 **principal component showing that sensors with noticeably negative loadings showed distinctly negative z-transformed minima.**

635



636

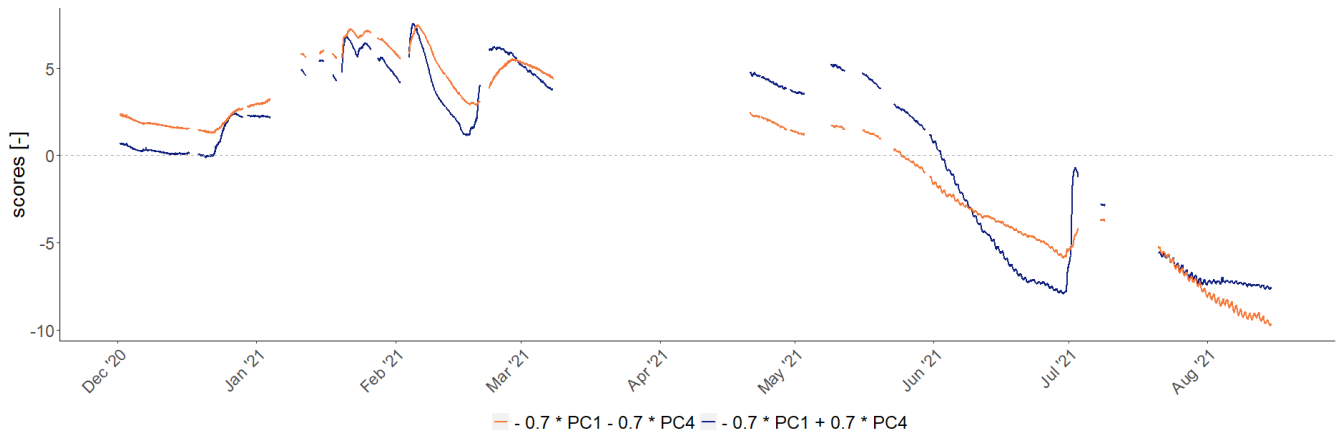
637 **Figure 8: Effect of the third principal component on modification of the general mean behaviour presented by the first principal**
 638 **component at the patchCROP landscape laboratory experiment, Tempelberg. The blue line represents deviations from mean soil**
 639 **moisture for time series with positive loadings on PC3 (majority of the time series) while the orange line represents deviations from**
 640 **mean soil moisture for time series with negative loadings on PC3 (part of the sensors in 0.9 m depth).**



642

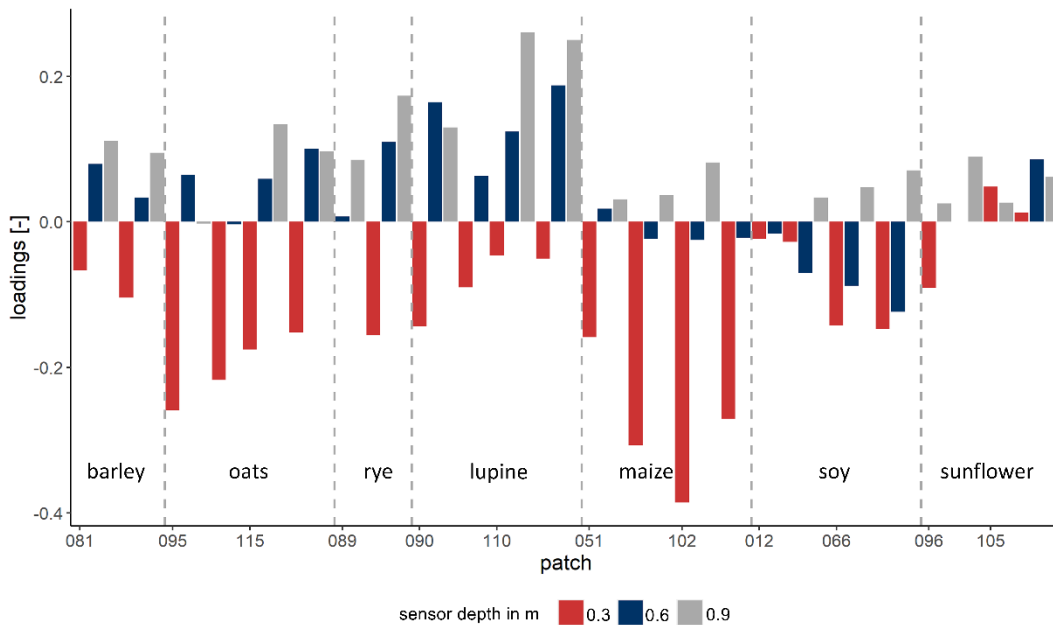
643 **Figure 9: Loadings of time series on the fourth principal component at the patchCROP landscape laboratory experiment,**
 644 **Tempelberg, Brandenburg, Germany showing mainly negative loadings for crop group A, positive loadings for crop group B and**
 645 **loadings with no clear pattern for crop group C. Bars represent individual time series grouped by patch ID, sorted by treatment**
 646 **group.**

647



648

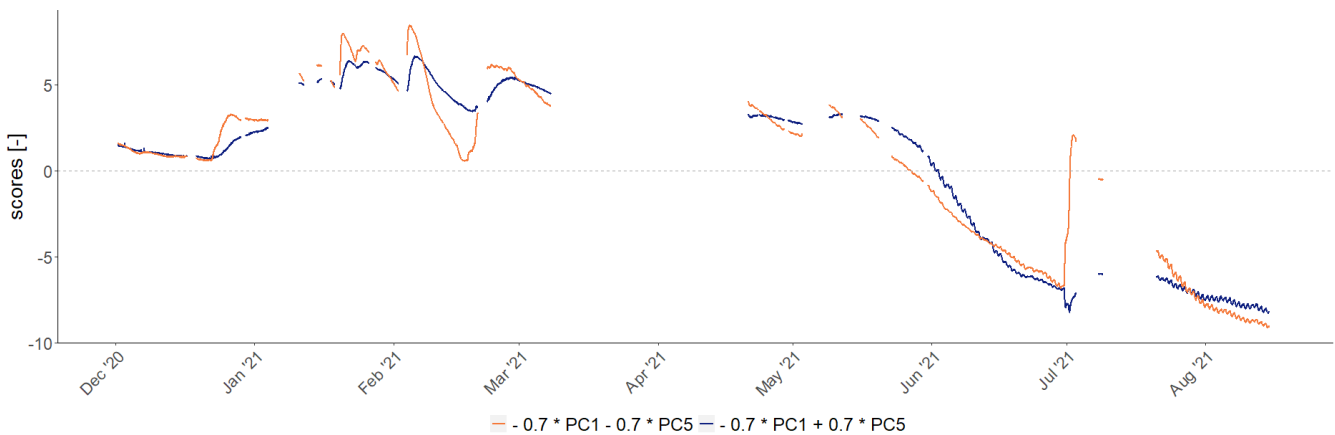
649 **Figure 10: Effect of the fourth principal component on modification of the general mean behaviour presented by the first principal**
 650 **component at the patchCROP landscape laboratory experiment, Tempelberg. The blue line represents deviations from mean soil**
 651 **moisture for time series with positive loadings on PC4 (single sensors of crop group A, all sensors of crop group B, and part of crop**
 652 **group C) while the orange line represents deviations from mean soil moisture for time series with negative loadings on PC4 (most**
 653 **sensors of crop group A and part of the sensors of crop group C).**



655

656 **Figure 11: Loadings of time series on the fifth principal component at the patchCROP landscape [laboratoryexperiment](#) showing a**
 657 **depth related pattern. Bars represent individual time series grouped by patch ID, sorted by crop.**

658



659

660 **Figure 12: Effect of the fifth principal component on modification of the general mean behaviour presented by the first principal**
 661 **component at the patchCROP landscape [laboratoryexperiment](#), Tempelberg. The blue line represents deviations from mean soil**
 662 **moisture for time series with positive loadings on PC5 (sensors in greater depth) while the orange line represents deviations from**
 663 **mean soil moisture for time series with negative loadings on PC5 (sensors in shallow depth).**

664

665

666 Table 1: Overview of crop rotation, sand content in the top 0.25 m soil depth and weed control for selected patches at the patchCROP
 667 landscape laboratory experiment, Tempelberg, Brandenburg, Germany.

Crop in winter season	Crop in summer season	Crop group	Sand content (in 1 m buffer zone around sensors) in %	Weed control	Patch ID
Winter barley		A	78.3	conventional	81
Winter oats		A	80.7	conventional	95
Winter oats		A	80.6	reduced	115
Winter rye		A	80.5	conventional	89
Fallow	Lupine	B	80.6	conventional	90
Fallow	Lupine	B	80.3	reduced	110
Phacelia	Maize	C	80.8	reduced	51
Phacelia	Maize	C	80.6	conventional	102
Phacelia	Soy	C	78.5	reduced	12
Phacelia	Soy	C	77.9	conventional	66
Phacelia	Sunflower	C	80.6	conventional	96
Phacelia	Sunflower	C	80.5	reduced	105

668

669 Table 2: Overview of normalized difference vegetation index (NDVI), surface temperature, and slope at the locations of analysed
 670 sensors at the patchCROP landscape experiment in Tempelberg, Brandenburg, Germany.

Crop	Patch ID	Sensor Position	NDVI 2021-05-20 [-]	NDVI 2021-05-31 [-]	NDVI 2021-07-06 [-]	Surface Temperature 2021-05-31 in °C	Slope in °
Winter barley	81	West	0.874	0.182	0.926	20.57	2.01
Winter barley	81	East	0.875	0.180	0.927	20.43	1.94
Winter oats	95	East	0.838	0.208	0.834	27.25	1.36
Winter oats	95	West	0.838	0.213	0.840	27.85	1.15
Winter oats	115	West	0.756	0.278	0.845	23.70	1.28
Winter oats	115	East	0.783	0.281	0.863	25.12	0.43
Winter rye	89	West	0.796	0.263	0.856	22.39	1.74
Winter rye	89	East	0.787	0.206	0.822	24.95	1.67
Lupine	90	West	0.185	0.395	0.710	26.31	1.40
Lupine	90	East	0.203	0.391	0.733	24.96	1.27
Lupine	110	West	0.090	0.563	0.635	26.98	1.88
Lupine	110	East	0.090	0.567	0.639	26.76	2.50

Maize	51	West	-0.099	0.654	0.181	35.44	0.82
Maize	51	East	-0.096	0.638	0.217	35.29	0.93
Maize	102	West	-0.077	0.714	0.175	37.88	0.88
Maize	102	East	-0.058	0.728	0.178	38.03	0.90
Soy	12	West	-0.107	0.748	0.166	34.87	1.71
Soy	12	East	-0.108	0.723	0.162	34.44	1.11
Soy	66	West	-0.115	0.730	0.144	35.09	2.40
Soy	66	East	-0.114	0.661	0.147	34.39	2.13
Sunflower	96	West	-0.109	0.816	0.211	33.76	0.59
Sunflower	96	East	-0.101	0.827	0.229	34.70	0.69
Sunflower	105	West	0.178	0.610	0.564	29.79	1.04
Sunflower	105	East	0.030	0.696	0.399	34.53	1.00

671

672 **Table 3: Statistical characteristics and interpretations of principal components 1 to 5 for soil moisture dynamics of selected patches**
673 **at the patchCROP landscape laboratoryexperiment, Tempelberg, Brandenburg, Germany.**

	PC1	PC2	PC3	PC4	PC5
Eigenvalue	46.25	10.89	2.60	1.43	1.06
Proportion of variance in %	72.27	17.01	4.06	2.23	1.65
Proportion of variance (cumulative) in %	72.27	89.28	93.34	95.57	97.22
Interpretation	Mean behaviour	Winter vs. summer crops	Subsoil texture	winter vegetation cover and influence of cover crops on soil <u>hydraulic properties</u>	Damping of the input signal
Prevailing driver	weather	crop	soil	crop and soil	soil

674

675 **Table 4: Pearson correlation coefficients between surface temperature and normalized difference vegetation index (NDVI) at the**
676 **patchCROP landscape laboratoryexperiment, Tempelberg, Brandenburg, Germany, and loadings of sensors in all depths or at single**
677 **depths, respectively, on the second principal component. All correlations were highly significant ($p < 0.01$).**

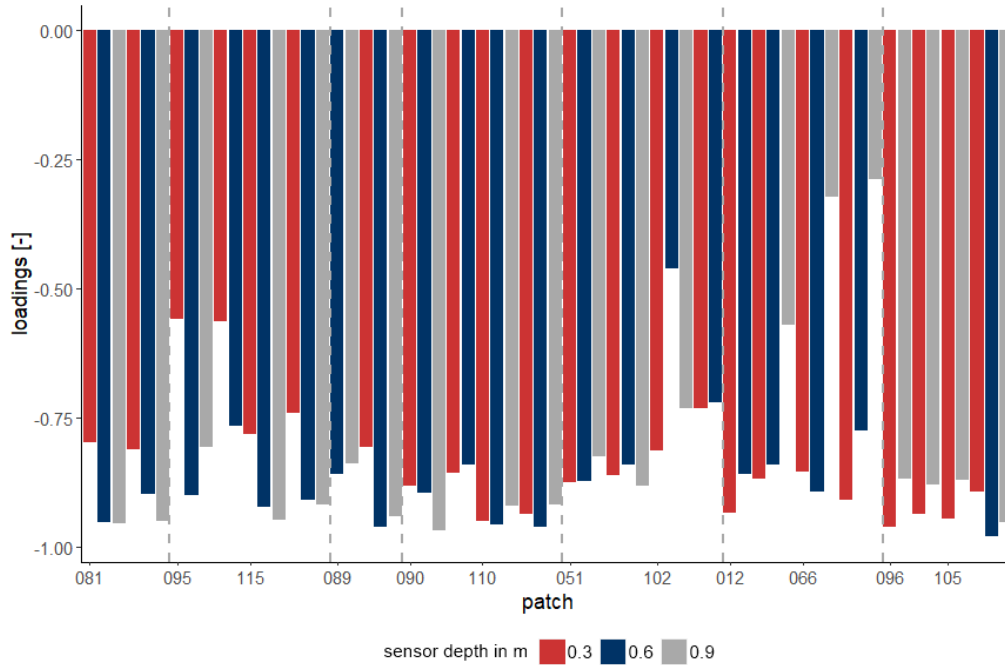
Variable	Sensors in all depths	0.3 m	0.6 m	0.9 m
Surface temperature	-0.853	-0.881	-0.909	-0.916
NDVI 2021-05-20	0.836	0.904	0.837	0.907

NDVI 2021-05-31	0.899	0.945	0.944	0.946
NDVI 2021-07-06	-0.860	-0.898	-0.917	-0.913

678

679

680 APPENDIX A



681

682 **Figure 13: Loadings of time series on the first principal component at the patchCROP landscape [laboratory experiment](#), Tempelberg,**
683 **Brandenburg, Germany. Bars represent individual time series grouped by patch ID and sorted by crop.**